Climate–Land Carbon Cycle Simulation of the 20th Century: Assessment of HadCM3LC C4MIP Phase 1 experiment.

Hadley Centre technical note 59

Chris Jones, Matthieu Warnier

2 Deceember 2004

Met Office

Climate–Land Carbon Cycle Simulation of the 20th Century: Assessment of HadCM3LC C4MIP Phase 1 experiment.

Chris Jones & Matthieu Warnier

November 2004.

1. Introduction

Interactions between climate and the carbon cycle have the potential to provide major feedbacks on climate change, but major uncertainties in the magnitude of these feedbacks persist (Cox et al., 2000; Friedlingstein et al., 2001, Friedlingstein et al., 2003, Jones et al., 2003 , Zeng et al., 2004b). The Coupled Climate-Carbon Cycle Model Intercomparison project (C4MIP) aims to investigate the plausible sensitivity of independent models driven by a common set of forcings.

The ultimate aim of C4MIP is therefore to perform a suite of simulations of 20th and 21st Century climate change including the atmospheric, terrestrial and oceanic components of the climate carbon cycle system. The comparison of a range of models will highlight areas of modelling uncertainty which contribute most to the spread of projected future carbon cycle behaviour. Validation of these experiments against climatological data may help to constrain the uncertainty.

Before embarking on an intercomparison of the fully coupled models, phase 1 of C4MIP will comprise simulations with only the atmospheric and terrestrial biosphere submodels coupled together. Ocean surface temperatures, sea-ice extent and depth and atmospheric carbon dioxide concentrations will be prescribed as boundary conditions. The simulations will cover only the 20th century, to allow the use of observational data for forcing and validation. In this experiment, the SSTs and sea-ice are prescribed from the HadISST climatology (Rayner et al., 2003) and atmospheric CO_2 is prescribed from Ice Core data and the Mona Loa record. Land use is held fixed at its 1900 state (Ramankutty and Foley, 1999; Goldewijk, 2001): there is no anthropogenic disturbance to land use. The vegetation cover is modelled dynamically by TRIFFID (Cox, 2001), a dynamic global vegetation model (DGVM).

In this report we asses the ability of the Hadley Centre's fully coupled climate carbon cycle model, HadCM3LC (Cox et al., 2001), to simulate the climate and terrestrial carbon cycle of the 20th century. Results are presented assessing many different aspects of the simulation from local to global spatial scales and annual to centennial temporal scales. First, we present an overview of the simulated climate and global mean changes in the terrestrial biosphere (section 2). We then compare the model with point-flux measurements from CarboEurope tower data (Aubinet et al., 2000; Valentini et al., 2003) in section 3. Section 4 presents an analysis of the interannual variability of the carbon cycle, in particular how it responds to the ENSO cycle, and then section 5 presents a comparison of present day carbon fluxes on a regional scale with the TransCom3 inversion estimates of Gurney et al. (2002). A breakdown of 20th century carbon fluxes by country is presented in section 6, and conclusions are given in section 7.

2. Overview of simulated climate and carbon cycle changes throughout the 20th Century

The simulation of the terrestrial carbon cycle will depend on the simulation of the climate. Given prescribed SSTs, sea-ice and atmospheric CO_2 it can be expected that global mean surface air temperature will closely follow observations, but regional differences in temperature and especially precipitation may adversely affect the model's ability to simulate biospheric changes during the 20th century. This section presents an overview of the main changes in simulated climate and carbon fluxes and stocks.

Climate

As expected, the model simulation is able to simulate the global annual mean surface air temperature over the sea to a high degree of accuracy compared with the climatology of Legates and Willmott (1990) (fig 2.1). However, there are some noticeable differences over land areas. This is especially noticeable over high land (such as the Himalayas and Greenland) where the model simulates too cold temperatures. There is in general, a cold bias of the model over most land area (fig 2.1, bottom panel). The larger errors over the Himalayas, Greenland and also the Saharan region are in areas where there is no (or very little) active biosphere and so this particular model deficiency will not have an impact on the simulation of the carbon cycle. Typically, errors in mid-latitudes are smaller than elsewhere with probably the most significant cold bias, in terms of simulation of the biosphere, being in the boreal regions.

With respect to precipitation, figure 2.2 shows the 1979-1999 annual mean precipitation rate from the CMAP climatology of Xie and Arkin (1997) compared with the same quantity from the model. Again, the overall pattern shows a good match of the model to the climatology, although the model has maybe too much tropical convection over the West Pacific and a too weak ITCZ over the equatorial Atlantic. When we focus on precipitation over land (fig 2.2, bottom panel) there is a small wet bias in the model (simulated mean land precipitation rate of 1.96 mm day^{-1} compared with 1.92 mm day^{-1} in the climatology). This wet bias is apparent over north-west North America, southern Africa, central and western South America, China and, to a lesser extent, western Europe. The model simulation is too dry in India and across the maritime continent, and also over north-east Amazonia, possibly due to the weak Atlantic ITCZ.

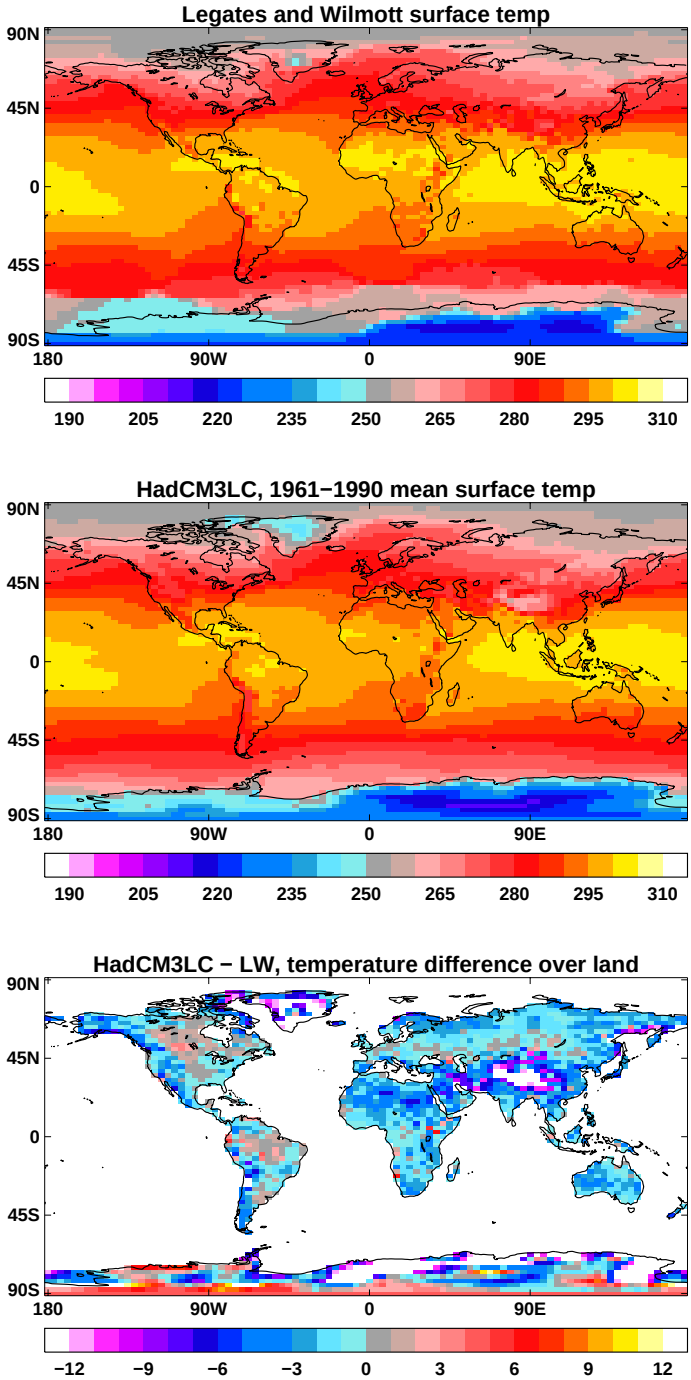

Figure 2.1. Maps of annual mean 1.5m surface air temperature (K). (a) Legates and Willmott climatology (1990); (b) HadCM3LC 1961-1990 mean simulated temperature; (c) Simulated minus climatological temperature over land.

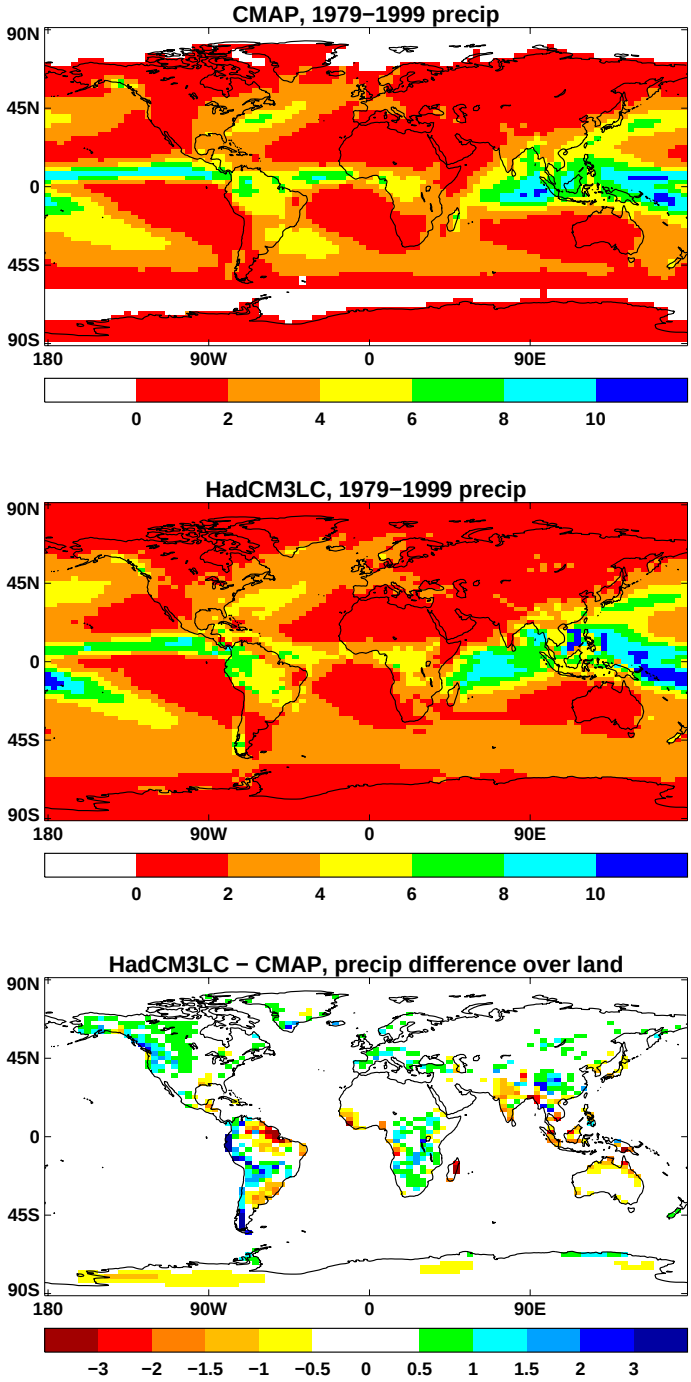

Figure 2.2. Maps of annual mean precipitation rate (mm day^{-1}). (a) CMAP climatology (1979-1999, Xie and Arkin, 1997); (b) HadCM3LC 1979-1999 mean simulated precipitation; (c) Simulated minus climatological precipitation over land.

Carbon Storage

Gross primary productivity (GPP) and ecosystem respiration (RE) both increase steadily at a similar rate during the 20th century (fig 2.3), increasing from approximately 120 GtC yr^{-1} at the start of the century to about 135-140 GtC yr^{-1} by the end.

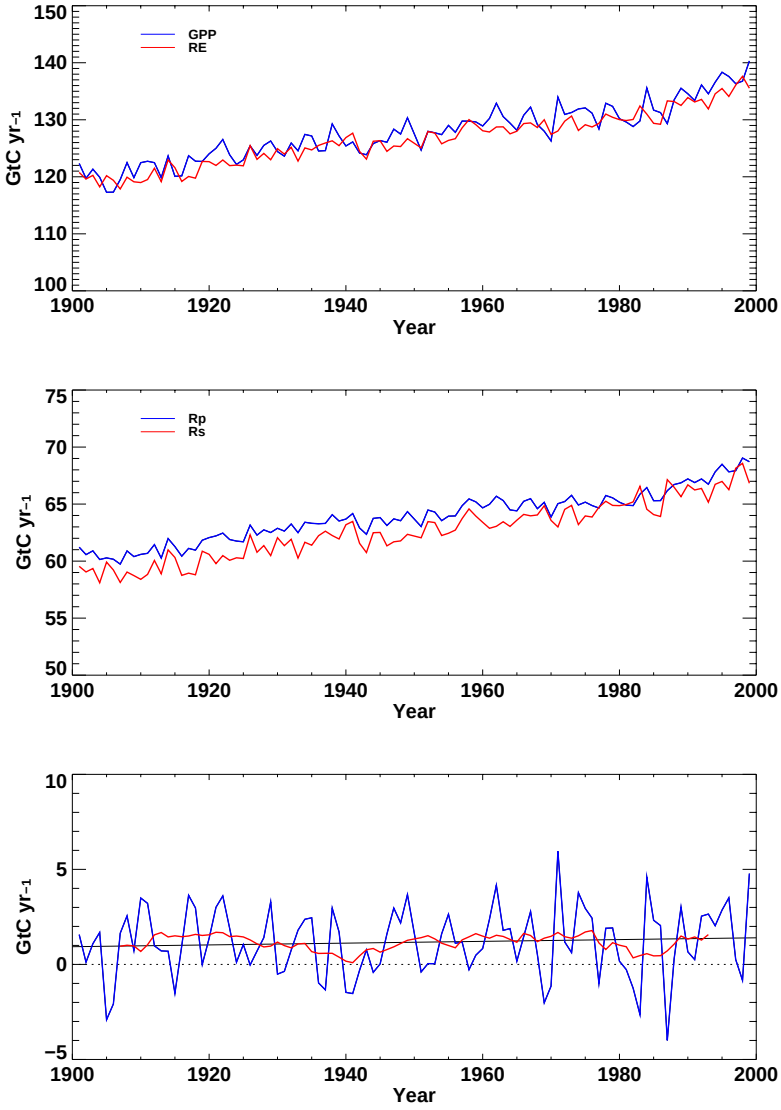

Figure 2.3. Simulated terrestrial carbon fluxes (GtC yr^{-1}) throughout the 20th century. (a) Gross primary productivity (GPP, blue line) and ecosystem respiration (RE, red line). (b) Components of ecosystem respiration: plant respiration (R_P, blue line) and soil respiration (R_S, red line). (c) Net ecosystem productivity (NEP = GPP – RE): annual mean (blue line), 11 year boxcar smoothing (red line), best fit linear trend (black line).

Simulated RE consists of contributions from plant and soil respiration (R_P, R_S respectively). The increase of RE is due to the increase at nearly the same rate of both R_P and R_S. It is apparent that R_S has a greater magnitude of interannual variability. This is likely because R_S interannual variability is driven predominantly by temperature whereas R_P interannual variability is dependent on both temperature and GPP (and hence on precipitation). Because temperature and precipitation often vary out of phase variability in R_P is consequently smaller.

GPP is generally slightly greater than RE and consequently there is a small but generally positive terrestrial carbon uptake throughout the 20th century (fig 2.3, bottom panel). This Net Ecosystem Productivity (NEP) has substantial interannual variability which is well correlated with the El Nino/Southern Oscillation (ENSO) as will be discussed in the section 4. The interannual variability in NEP is large compared with the changes in its mean, which makes detection of a trend uncertain. A linear regression gives a best fit trend of 0.5±1.2 GtC yr^{-1} $century^{-1}$ – in other words, NEP has increased from about 0.9 GtC yr^{-1} to 1.4 GtC yr^{-1} over the 20th century, but this trend is not distinct from zero in a statistically significant sense.

Uptake of carbon by the biosphere during the 20th century is apportioned between the soil and vegetation carbon stocks. The initial global soil carbon stock (1138 GtC) is approximately twice as big as the vegetation carbon stock (565 GtC) but their total increases over the 20th century are similar, reaching 1194 GtC and 623 GtC by the present day (fig 2.4). Soil carbon increases more quickly than vegetation carbon in the early part of the century, but slower during the final two decades.

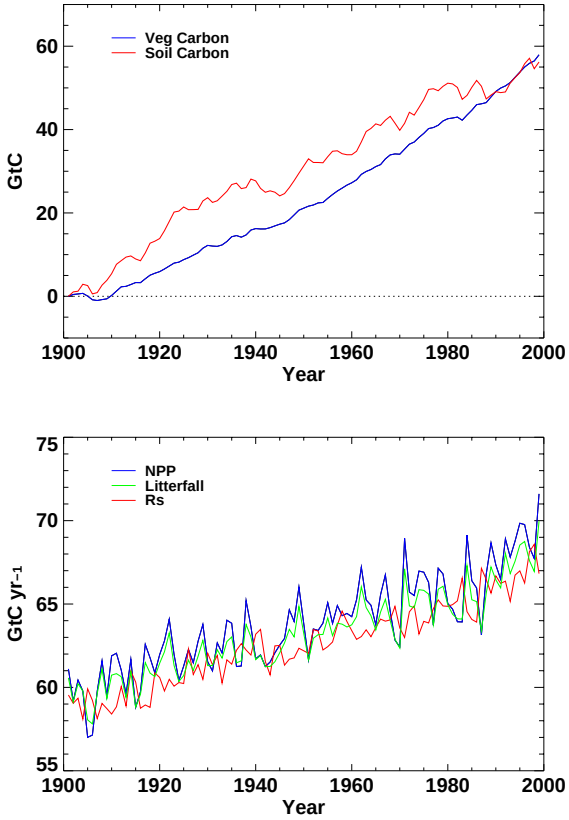

Figure 2.4. (a) Simulated changes in soil (red line) and vegetation (blue line) carbon (GtC) relative to their 1901 values. (b) NPP (blue line), litterfall (green line) and R_S (red line), in GtC yr^{-1}, throughout the 20th century.

Storage in vegetation carbon is driven by the difference between NPP (GPP-R_P) and the vegetation to soil turnover (litterfall). Storage in soil carbon is driven by the difference between the litterfall input and soil decomposition (R_S). Figure 2.4 (bottom panel) shows that throughout the 20th century, NPP > litterfall > R_S, with litterfall closer to NPP during the first half of the century resulting in more rapid carbon storage in the soil, but by the end of the century litterfall is now closer to R_S resulting in more rapid accumulation of carbon in the vegetation. The reason for this change in the apportioning of NEP is beyond the scope of this report, but may be very

important. This partitioning is thought to be one of the important controls over the future size of the carbon cycle feedback, and one reason why different models simulate different feedback strengths (Friedlingstein et al., 2003).

Vegetation Cover

Being a DGVM, TRIFFID can simulate dynamically changes in vegetation cover. TRIFFID simulates the competition between 5 plant functional types (PFTs): broadleaf and needleleaf trees, C3 and C4 grasses and shrubs. The absence of vegetation is assumed to be bare soil. It should be remembered that there is no changing land use in this experiment, so the simulated changes are the natural changes of the vegetation to the changing climate and CO_2 concentration.

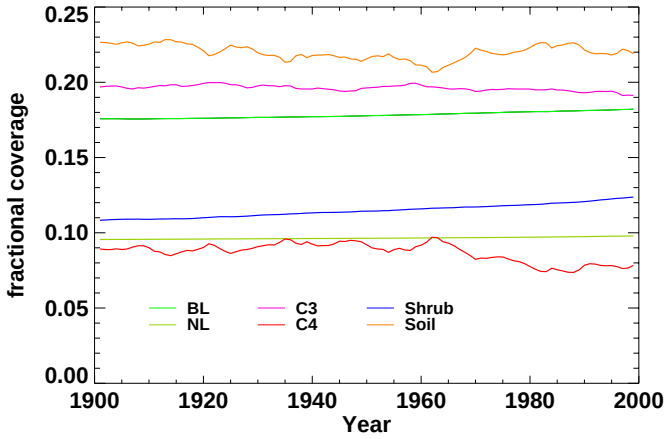

Figure 2.5. Vegetation fraction for each PFT. "BL": broadleaf trees, "NL": needleleaf trees, "C3": C3 grass, "C4": C4 grass.

Globally, there are only very small changes in the mean coverage of each PFT (fig 2.5). C3 grasses and needleleaf trees remain at about the same fraction. Broadleaf trees and shrubs increase their fractions whereas bare soil and C4 grasses are reducing in cover. C4 grass and bare soil have greater variability than the other PFTs and they seem to be anticorrelated. C4 grasses often occupy hot and/or arid areas and so their evolution is strongly linked to that of bare soil extent. There are big fluctuations of both in India and Australia: as one increases the other decreases.

However, regionally there are some changes in vegetation. For example, broadleaf trees are increasing in their coverage in Amazonia at the expense of C4 grass there (fig 2.6), and shrubs are increasing their coverage in Boreal Asia at the expense of C3 grass there (fig 2.7, top 2 panels). These changes in the Boreal regions are consistent with the evidence of Sturm et al. (2001) who describe increased shrub coverage in Alaska compared with aerial photographs taken between 1948 and 1950. Zhou et al. (2001) and Tucker et al. (2001) also present satellite observed NDVI data which suggests that boreal regions have greened over the past two decades due to increased growing season length as the temperature increases. The model simulates increased leaf area index (LAI) in the north during the course of the century (fig 2.7, bottom 2 panels).

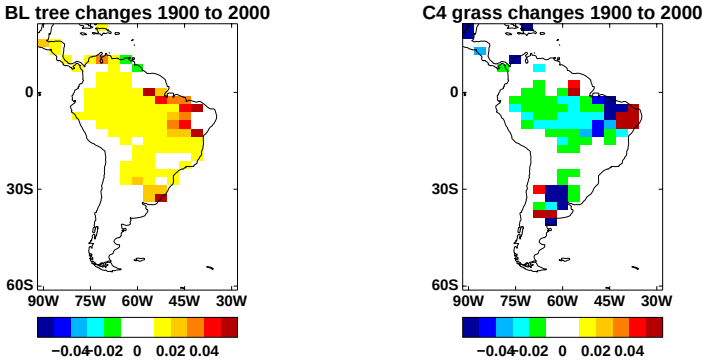

Figure 2.6. Changes in the fractional coverage of broadleaf trees and C4 grasses in South America from 1900 to 1999.

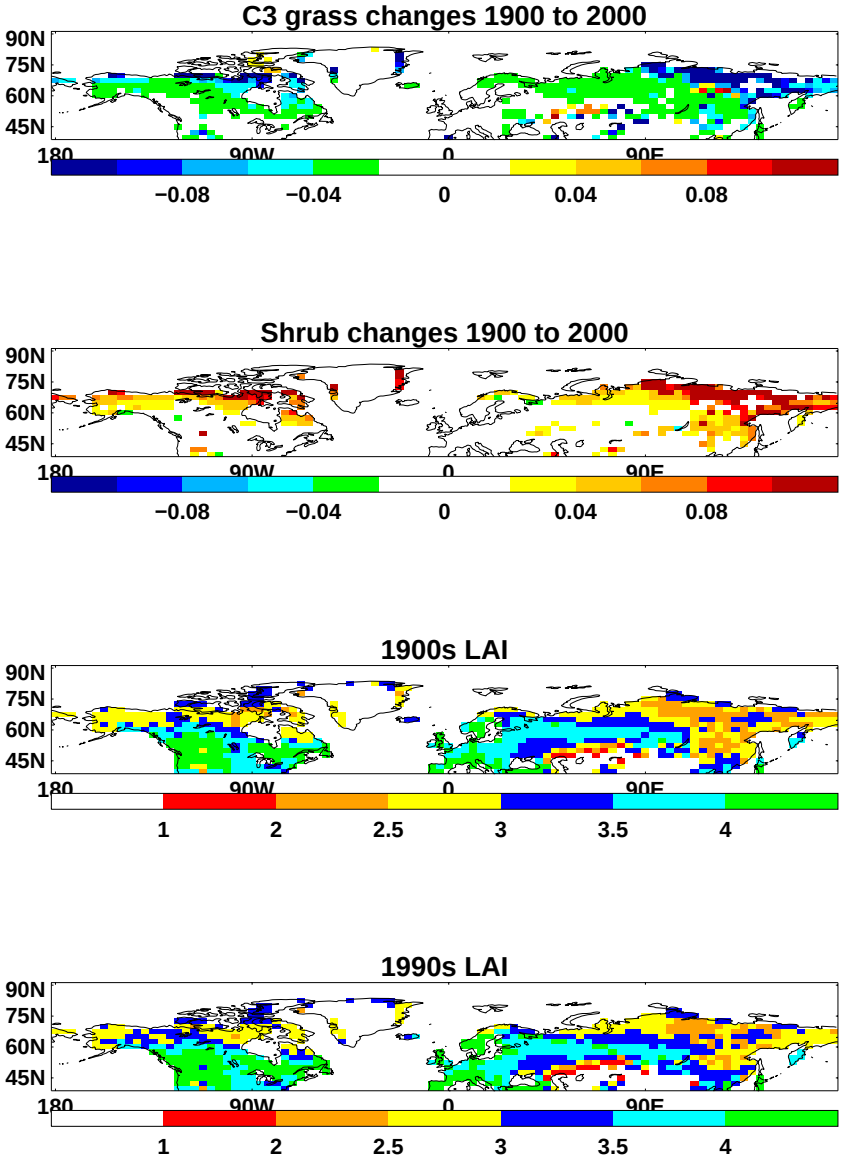

Figure 2.7. Changes in the fractional coverage of (a) C3 grass trees and (b) shrubs in high latitudes from 1900 to 1999. Simulated leaf area index (LAI) for (c) 1900 and (d) 1990s.

3. Comparison with CarboEurope flux data

In recent years there has been a significant increase in direct measurement of net biospheric CO_2 flux from a growing network of flux tower sites across Europe (CarboEurope: Aubinet et al., 2000; Valentini et al., 2003). This section presents a comparison of model results with measured fluxes from 14 CarboEurope sites from Sweden to Italy, between 1997 and 2000 (table 3.1).

Site identifier	Site name and country	latitude	longitude	Site elevation (m)	Model elevation (m)	Site land cover	Model tree cover (%)	Model grass cover (%)
FL	Flakaliden, Sweden	64°N	19°E	315	326	coniferous	67	15
HY	Hyytiälä, Finland	62°N	24°E	170	29	conifer forest	91	7
NO	Norunda, Sweden	60°N	17°E	45	181	coniferous	83	11
AB	Griffin (Aberfeldy), United Kingdom	57°N	4°W	340	220	coniferous	35	55
SO	Soroe, Denmark	55°N	12°E	40	13.5	hardwood forest	40	46
LO	Loobos, The Netherlands	52°N	6°E	25	62	coniferous	11	76
TH	Tharandt, Germany	51°N	14°E	380	113	coniferous forest	54	34
BR	Brasschaat - De Inslag Forest, Belgium	51°N	5°E	16	128	mixed forest	2	90
VI	Vielsalm, Belgium	50°N	6°E	450	128	mixed forest	2	90
WE	Weidenbrunnen , Germany	50°N	12°E	780	412	coniferous forest	60	30
HE	Hesse , France	49°N	7°E	300	128	hardwood forest	2	90
BO	Le Bray, France	45°N	1°W	60	234	coniferous	23	71
CP	Castelporziano, Italy	42°N	12°E	3	207	hardwood forest	77	9
CL	Collelongo, Italy	42°N	14°E	1550	207	hardwood forest	77	9

Table 3.1. Description of the CarboEurope sites used for this comparison. The list here has been ordered by latitude to match the order in figures 3.1 to 3.3.

The following comparison of model versus observed point fluxes must bear in mind the difficulties in making such a comparison. Firstly, a gridbox mean quantity at a resolution of several hundreds of kilometres may be very different to a locally measured flux representative of just a few kilometres. Second, the elevation and topography of the site may contribute to features of the local flux which cannot be captured by the broad scale of the model. Maybe most importantly though, there are issues to do with both the history of land-use at the site and the current land-management practices which may mean that the processes responsible for the local fluxes (such as aforestation or reforestation) cannot be simulated by the C4MIP

experiment which does not include land-use change. Thornton et al. (2002) claim that land-use history is the single most important factor in determining local NEE, with climate and CO_2 changes secondary. Finally, were it to be established that there are differences between the model and the local measurement, it maybe difficult to find the reason for them – are they due to climatic errors in the model, errors in the simulated land-cover at that point or errors in the simulation of the carbon fluxes for that vegetation? In Europe in particular there is great heterogeneity – forested regions rarely occupy the 200km x 300km size areas of the model gridboxes. Also, European forests are often actively managed and thus won't exhibit the purely natural response which is what the model is attempting to simulate.

The analysis performed here only considers annual mean data. While it may be interesting to also look at seasonal or even monthly timescales, it was felt that the inherent difficulties in comparing model with point data meant that such a detailed comparison would be difficult to interpret and may not yield any more information than the annual data considered here.

It should also be noted that it is the net flux (NEP) which is the quantity that is directly observed by the flux measurements. Apportioning this into growth (GPP) and respiration (RE) is done based on several assumptions. First, a relationship between respiration and temperature is derived for night time fluxes (when GPP will be zero). This is assumed to hold during the daytime (i.e. plant respiration follows the same temperature dependence as soil respiration) in order to derive the respiration and growth components of the measured net flux. This approach introduces considerable uncertainty into the GPP and RE estimates and so it is important to remember that they are not direct "observations".

When we look across the flux data, two inconsistencies are apparent. Firstly, simulated NEP is generally much smaller in magnitude than observed (fig 3.1). Secondly, RE is nearly always greater in the model than in the measurements (fig 3.2). There is no such apparent bias in modelled GPP (fig 3.3). Although local discrepancies in GPP can be large, they are sometimes overpredicted and sometimes underpredicted by the model.

It is interesting to note that some sites occupy the same model gridbox, which allows us to asses the variability of measured fluxes on a small scale and to estimate to what extent the model can be expected to accurately simulate the measured fluxes at a given site. In particular, BR, HE and VI lie in the same model gridbox in north-eastern France/Belgium. In common with many of the sites, the model simulates a greater respiration flux (about 1700 to 1900 $gCm^{-2}yr^{-1}$) than is measured (all three sites estimate respiration fluxes of around 800 to 1300 $gCm^{-2}yr^{-1}$). The sites report similar GPP values to each other (typically 1000 to 1400 $gCm^{-2}yr^{-1}$), and again the model simulates greater magnitude of fluxes, with GPP ranging between 1600 and 1800 $gCm^{-2}yr^{-1}$. These differences in the gross fluxes translate into very large differences in the observed net fluxes. BR reports a source of 200 $gCm^{-2}yr^{-1}$, while VI (which has the same mixed forest land cover) reports a strong sink of 500 $gCm^{-2}yr^{-1}$. HE, with hardwood forest, lies between them, reporting a sink of 100-300 $gCm^{-2}yr^{-1}$. The model (which simulates land cover as predominantly grass) simulates a weak source of less than 100 $gCm^{-2}yr^{-1}$. Although the difference in simulated land cover by the model makes it difficult to compare model with observations at this point, it is the intra-observational comparison which is interesting. Small differences in the gross fluxes at the sites lead to very different net carbon balance. This is a very good

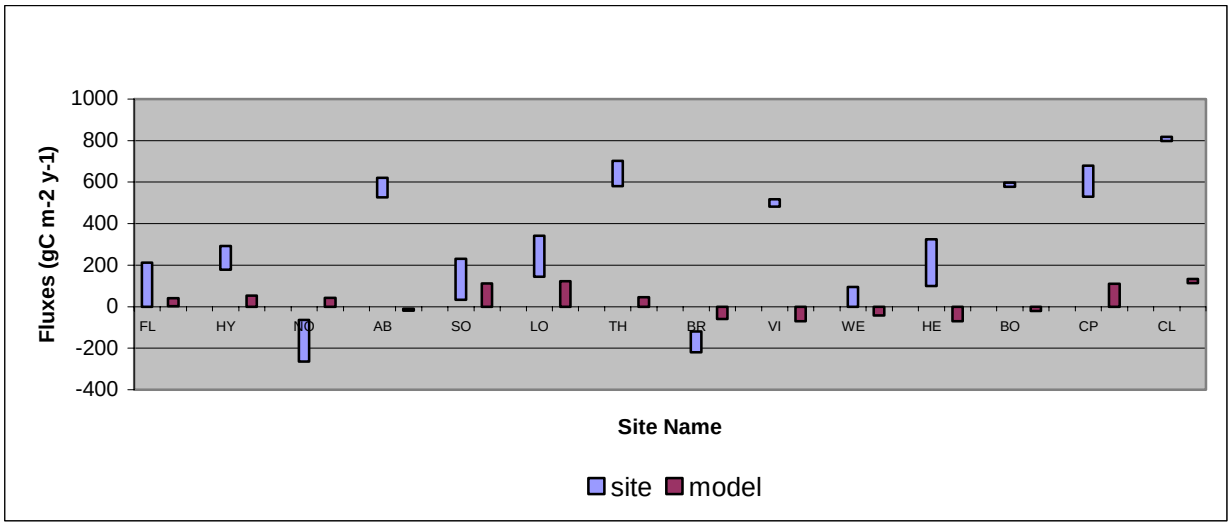

Figure 3.1. Annual NEP values for the CarboEurope sites listed in table 3.1 (blue bars) along with model NEP from the corresponding gridbox (red bars). The sites are ordered by latitude (northernmost to the left). The bars represent the maximum and minimum values reported by the sites during the years 1997-2000.

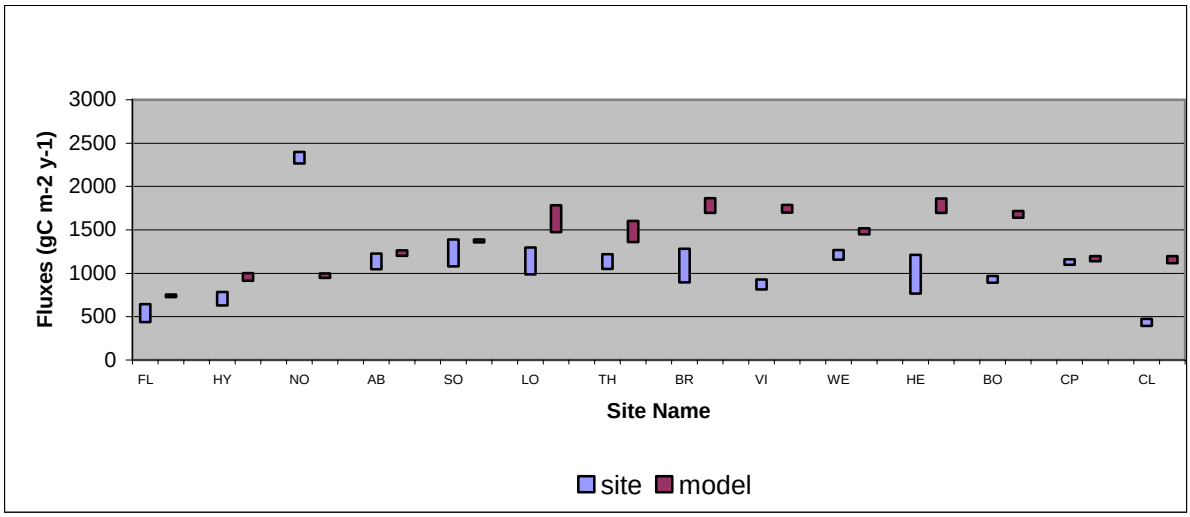

Figure 3.2. As for fig 3.1 but for ecosystem respiration (RE).

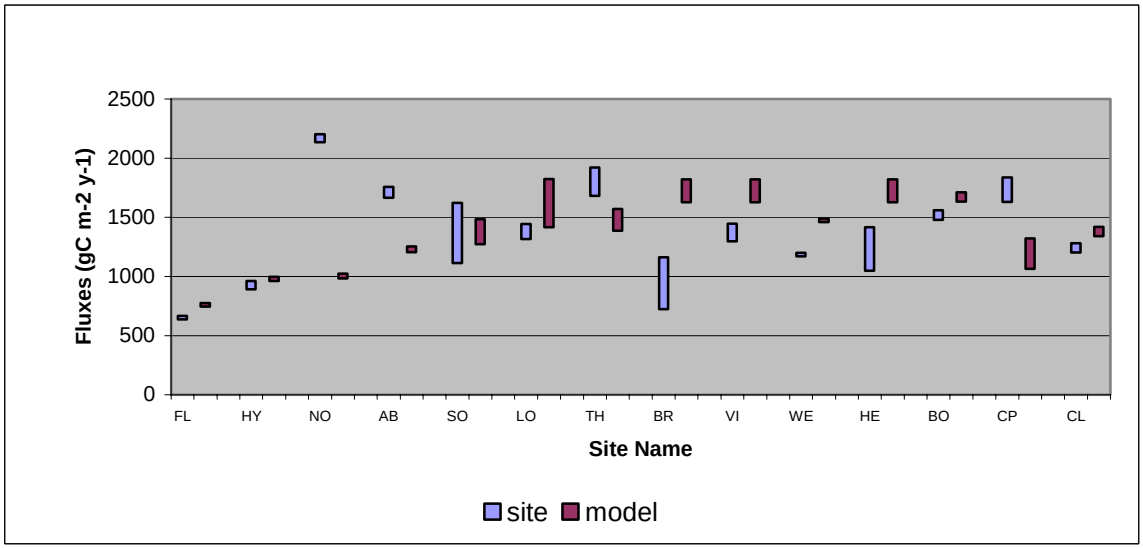

Figure 3.3. As for fig 3.1 but for gross primary productivity (GPP).

illustration of the difficulties of simulating the carbon balance between 2 large and uncertain fluxes, and illustrates the dangers of expecting too close an agreement between model and flux towers: it may not be possible, or even desirable, for such a global model to match observations precisely.

Given the potential differences in both land cover and land use history between the model and measurement sites, and the lack of representivity of point flux measurements over gridbox areas, GPP and to a lesser extent RE show reasonable agreement. Possibly the main persistent difference between the simulated and measured fluxes is the tendency for the model to simulate too great values of RE. This is illustrated both on a point by point basis (fig 3.2) and also, but less so, for the relationship between RE and temperature (discussed below, and shown in fig 3.4). The reason for this bias is not clear, although the relationship between RE and temperature indicates that it is not entirely due to incorrect temperature sensitivity of respiration. It may be due to non-representivity of the measurement site over the corresponding gridbox, or more likely the different land use histories between the model and the measurement site leading to different stores of vegetation and soil carbon. However, it is not clear why this discrepancy is coherent across so many of the sites. It is not possible to tell from the observations how RE is apportioned between plant and soil respiration.

Because NEP is the small residual of two large, opposing fluxes, it is very difficult for the model to capture the signal in the measurements. This is illustrated by the previous discussion of the very different behaviour of the 3 sites which occupy the same model gridbox. There appears to be a tendency in the measured NEP values to show a European wide carbon sink. This is not captured by the model. Hence it is likely that this sink is not due to climatic changes or CO_2 fertilisation (which could be simulated by the model). Rather land-use change history and land management practices are the more likely explanations.

For a simple comparison of fluxes at a given point it is not straightforward to determine whether any discrepancy is due to climatic or carbon cycle differences in the simulation. To try to avoid this complication we examined the behaviour of the modelled fluxes as a function of temperature and precipitation. GPP and RE are both strongly dependent on temperature and GPP also on precipitation. Figure 3.4 shows the modelled and observed dependence of RE on temperature and figures 3.5 and 3.6 show the dependence of GPP on temperature and precipitation respectively.

It can be seen in fig 3.4 that RE increases with temperature in both the model and observations, although modelled values for a given temperature tend to be greater than the equivalent measured value. There are insufficient data to determine the nature of observed sensitivity of respiration to temperature. There are also a handful of points for both the model and observations which lie at high temperatures but do not have high respiration rates. We have not examined the reason for this, which could be due to local precipitation rates.

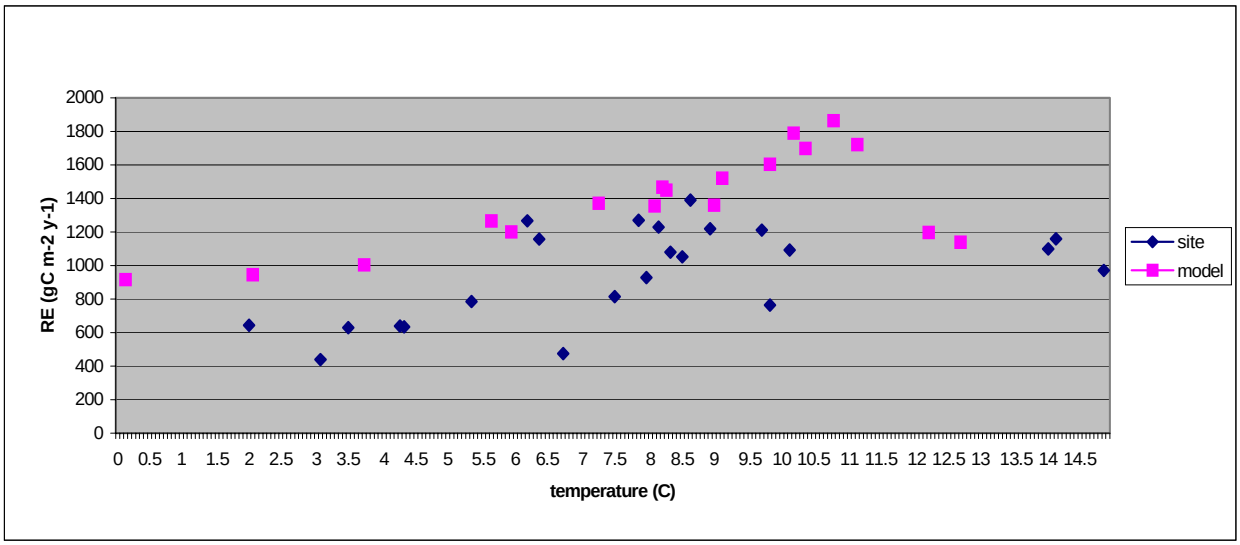

Figure 3.4. Dependence of annual mean ecosystem respiration on annual mean temperature for measured (blue) and model (red) fluxes.

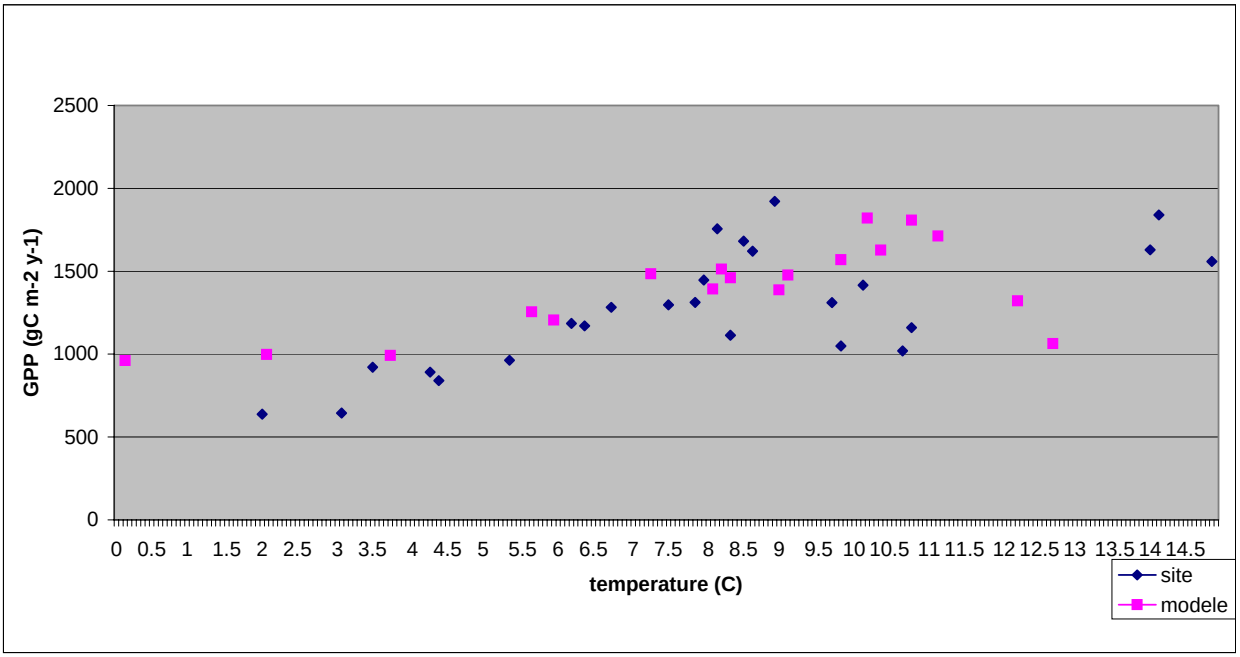

Figure 3.5. Dependence of annual mean productivity on annual mean temperature for measured (blue) and model (red) fluxes.

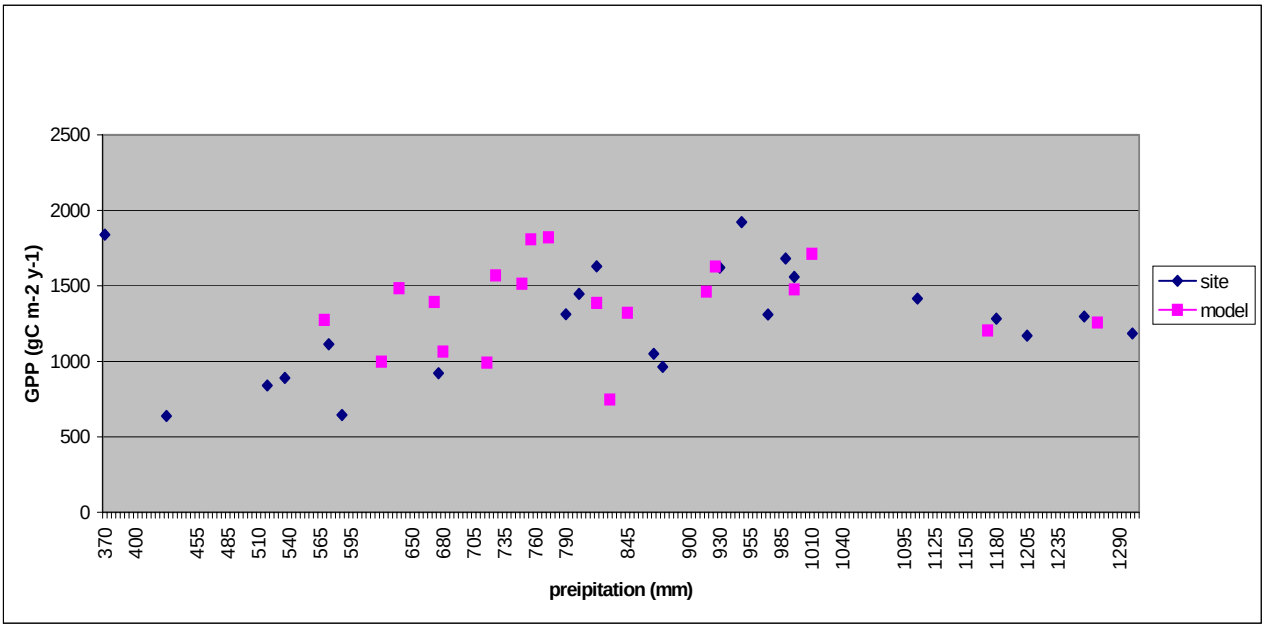

Figure 3.6. Dependence of annual mean productivity on annual total precipitation for measured (blue) and model (red) fluxes.

It can also be seen that GPP is strongly related to both temperature and precipitation (figs 3.5 and 3.6 respectively). GPP appears to increase approximately linearly with temperature over this range although the measured GPP appears to exhibit a greater sensitivity than in the model. GPP also increases with precipitation except for a few points at high precipitation values (both simulated and measured) which again may be due to factors other than the precipitation amount. The model shows very good agreement to the observed response of GPP to precipitation.

Given the difficulties in direct side-by-side comparison of model against flux measurements, especially in the absence of land-use changes in the model, it is these comparisons of the climatic influence on the fluxes which prove the most useful. The model appears to capture the main features of the observed dependence of GPP and RE on climate.

4. Carbon cycle response to ENSO

During El Nino events there are both higher temperatures and reduced precipitation over much tropical land area and, conversely, temperatures are lower and precipitation higher during La Nina events. Consequently NEP is reduced during El Nino and enhanced during La Nina in the tropics, especially in South America. Figure 4.1 shows the mean terrestrial flux to the atmosphere for a composite of two El Nino years (1982 and 1997) and two La Nina years (1955 and 1984). The pattern of response is similar to that found by Jones et al. (2001) in the fully coupled version of HadCM3LC. Minor differences include the fact that Australia and central Eurasia are sources of carbon here during El Nino events compared with weak sinks in Jones et al. (2001), and tropical Africa is a sink here compared with a source in Jones et al. (2001). In La Nina years, South Eastern USA is a sink here compared with a sink in Jones et al. (2001).

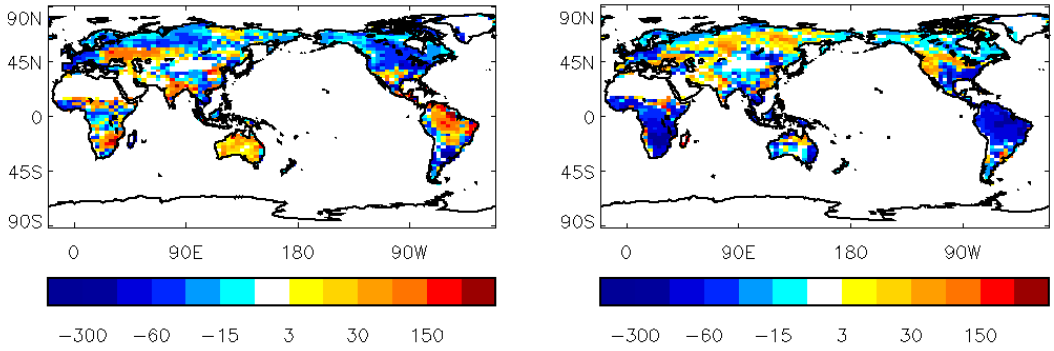

Figure 4.1. Composite annual mean terrestrial flux to the atmosphere (i.e. –ve of NEP, in $gCm^{-2}yr^{-1}$) for (a) two El Nino events (1982 and 1997) and (b) two La Nina events (1955 and 1984). Units and colour scale are chosen to be comparable with the results from the fully coupled model shown in figure 9 of Jones et al. (2001).

Previous studies describe (Keeling et al., 1995; Jones et al., 2001; Prentice et al., 2001) there is a strong anticorrelation between the Nino3 index and the global mean NEP (fig 4.2). Most of the global NEP variability is due to the tropical NEP, in agreement with Zeng et al (2004a). There are however significant differences between global mean and tropical NEP in the early 1980s and early 1990s perhaps due to significant carbon uptake in high latitudes following the large volcanic eruptions of El Chichon in 1982 and Mt. Pinatubo in 1991 (Jones and Cox, 2001; Lucht et al., 2002).

In the tropics, which are the greatest contributor to global NEP variability, precipitation and temperature are anticorrelated leading to an anticorrelation between soil respiration and NPP (fig 4.2, bottom panel). Hence both respiration and NPP anomalies act in the same sense generating large variability in NEP. Outside the tropics, local variations in temperature and precipitation cause local anomalies of respiration and NPP of similar magnitude per unit area to those in the tropics but because they lack large scale coherence and do not always act in the same sense, their effects often cancel and they do not contribute so significantly to the global total. This is in agreement with “conspiracy” theory of Zeng et al. (2004a).

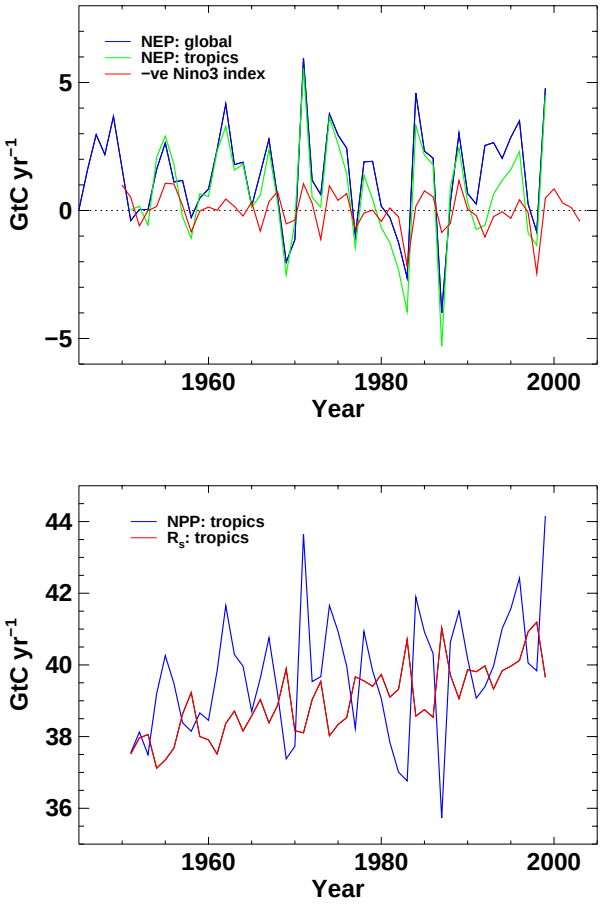

Figure 4.2. Simulated tropical behaviour of carbon fluxes. (a) Global mean and tropical mean NEP and -Nino3 index (negative of Nino3 index is plotted to better show the negative correlation between El Nino and NEP). (b) 20th Century soil respiration (R_S) and Net primary productivity (NPP) in the tropics.

As has been noted by previous studies (e.g. Keeling et al., 1995; Bousquet et al., 2000; Jones et al., 2001) the dominant contribution to interannual variability in the carbon fluxes to the atmosphere comes from land, with ocean fluxes of opposite sign but smaller magnitude. Hence it could be expected that the terrestrial carbon fluxes from this experiment should be able to explain much of the observed interannual variability in atmospheric CO_2 concentration. Figure 4.3 shows the relationship between terrestrial carbon flux (-NEP) and year-to-year changes in the atmospheric CO_2 at Mauna Loa. There is a high degree of agreement between the two in terms of the phase of positive and negative changes, although the simulated flux tends to be of greater magnitude than the observed change in CO_2. This would be expected to some degree if interannual variability in the ocean flux due to ENSO activity is largely opposing the terrestrial flux, although the magnitude of the cancellation is uncertain (Keeling et al., 1995; Francey et al., 1995). Two periods are apparent where there is a decoupling of the two timeseries – the early 1980s and the mid 1990s. These periods coincide approximately with the volcanic eruptions of El Chichon and Mt Pinatubo discussed above. It is possible that they may be caused by non-climatic influences of the eruption such as a change in the proportion of direct to diffuse light that reaches the vegetation (Gu et al., 2003) or stimulation of ocean uptake by iron rich dust deposition from volcanic ash. It is also likely that the short term atmospheric cooling

caused by the volcanic aerosol is not fully captured by the SST forcing and therefore cannot be simulated by a model without atmospheric aerosol radiative forcing. However, the two anomalous periods are of opposite sign, with simulated fluxes much greater than observed CO_2 changes in the 1980s and much smaller in the 1990s. Hence the reason for these anomalies is not yet known.

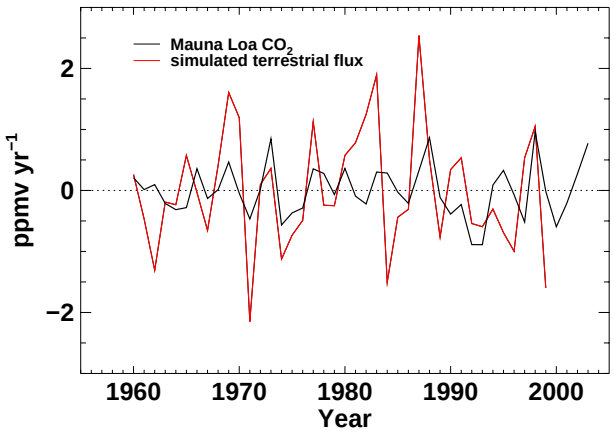

Figure 4.3. Interannual changes in atmospheric CO_2 concentration (ppm yr^{-1}) measured at Mauna Loa (black line) and simulated terrestrial carbon flux (ppm yr^{-1}, red line). For ease of comparison, both curves have been shifted to lie on top of each other by removing their mean over this period.

5. Comparison with CO_2 Inversion studies

The global carbon budget is reasonably well constrained by atmospheric trends of CO_2 and measurements of O_2:N_2. There are also accurate measurements of local ecosystem carbon balance from eddy covariance flux measurements, but comparison of these with GCM output is problematic – as discussed in section 3. However, there remains very little experimental information on carbon budgets at regional scales (i.e. on scales from several hundreds of kilometres up to continental areas). It is these scales which coupled climate carbon cycle GCMs could be expected to capture, but for which little directly measured validation data exists. Further, what data there are relies to some degree on modelling – such as the atmospheric transport models used in inversion studies.

In this section we make a comparison between the simulated land-atmosphere carbon flux and estimates from the TransCom3 project (Gurney et al, 2002) which is an intercomparison of Atmospheric CO_2 inversion models. Such methods attempt to take the observed atmospheric distribution of CO_2 concentration and model its evolution "in reverse" to see where it comes from – thus they can estimate regional sinks and sources which are consistent with the observed CO_2 and the modelled atmospheric circulation.

We repeat the comparison of Jones et al. (2003) of HadCM3LC experiments against the Gurney et al. (2002) estimates, with an extra result added from the current C4MIP experiment. The other experiments shown include the original coupled climate-carbon cycle experiment (Cox00: Cox et al, 2000) and two experiments which include climate forcing by anthropogenic sulphate aerosol and natural forcings of solar and volcanic variability: "ALL" (which has the same CO_2 emissions as Cox00) and "ALL70" which has revised land-use emissions (for more details, see Jones et al., 2003). All of these other experiments are with the fully coupled version of HadCM3LC as opposed to the C4MIP experiment which comprises just the atmospheric and terrestrial components and is driven with observed CO_2 and SST data.

One source of uncertainty in this comparison is that none of the model experiments account for land-use change in the calculation of NEP, so a land-use component must be added to the model results to enable comparison with the inversion estimates (which inherently include all sources and sinks of CO_2). Here, a flux of 1.3 GtC yr^{-1} to the atmosphere has been assumed uniformly over the tropics along with a flux of -0.4 GtC yr^{-1} north of 20^oN, giving a global mean land-use flux assumed at 0.9 GtC yr^{-1}. However, the magnitude of land-use change carbon fluxes are not well known with any regional accuracy. Hence it is possible that some of the regional discrepancies between modelled fluxes and inversion estimates are due to uncertainties in the assumed land-use flux added to the model results.

A further source of uncertainty is due to the fact that the period of measurements is directly after the Mt. Pinatubo eruption. It is likely that this had a significant impact on the global terrestrial carbon cycle both in terms of the climatic and non-climatic effects (such as via diffuse light or ocean fertilisation). Hence some of the discrepancy between the model and inversion results may be attributable to the eruption.

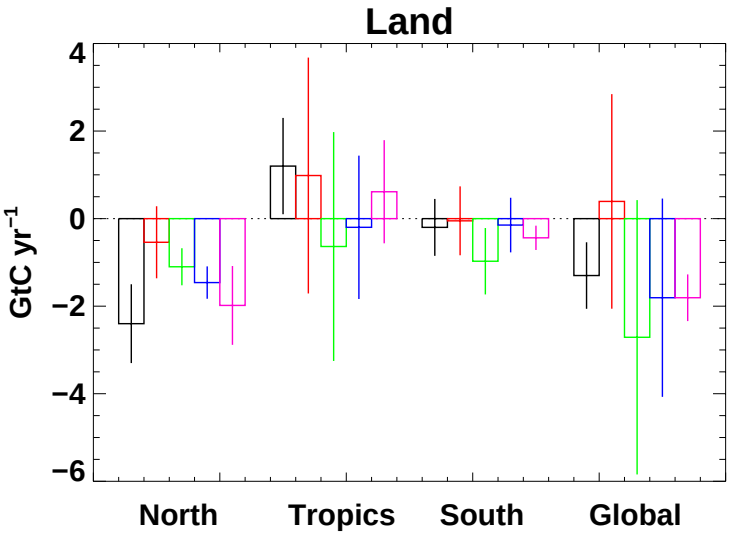

Figure 5.1. Land to Atmosphere global and semi-global fluxes for the period 1992-1996. Black rectangles represent estimated fluxes from the inversion study of Gurney et al. (2002). Coloured rectangles represent model results: Cox00 (red), ALL (green), ALL70 (blue), C4MIP (pink). The black lines represent the inversion study uncertainty. The coloured lines represent model interannual variability during the period.

The C4MIP experiment agrees with the global and semi-global TransCom3 estimates more closely than the other model experiments (fig 5.1), and well within the error bars of the inversion and the variability of the model.

This is also generally true for the regional estimates (fig 5.2). In temperate North America, Europe and Tropical Asia the C4MIP results are much closer to the inversion estimate than the other model experiments. Given that all the simulations use the same terrestrial carbon cycle model, it may be assumed that the improved simulation of the climate due to the SST forcing is most important in these regions.

It is interesting that the inversion results estimate a *source* for Boreal North America where the models consistently simulate a *sink*. However, the inversion estimate is quite uncertain, with error bars which span zero.

Both in Boreal Asia and South Africa there is general good agreement between all the model runs and the inversion estimate. It is not known why the terrestrial carbon balance of Boreal Asia is simulated much closer to the inversion estimates than that of Boreal North America.

In each of tropical America, South America and North Africa there is very large uncertainty in both the inversion data and the simulated fluxes. This is likely due to the fact that these are the regions whose climate is most strongly affected by ENSO. There is a suggestion that the model results broadly agree with the inversion data in these regions, but the noise is greater than the signal. The C4MIP experiment in particular seems to match the central inversion estimate well.

Temperate Asia and Australia are the two regions where the model results and inversion estimates differ most and also where the C4MIP results noticeably fail to improve the simulation. In fact, Australia is the only region where the C4MIP and inversion error bars do not overlap, with Gurney et al. estimating a source and the C4MIP experiment a sink.

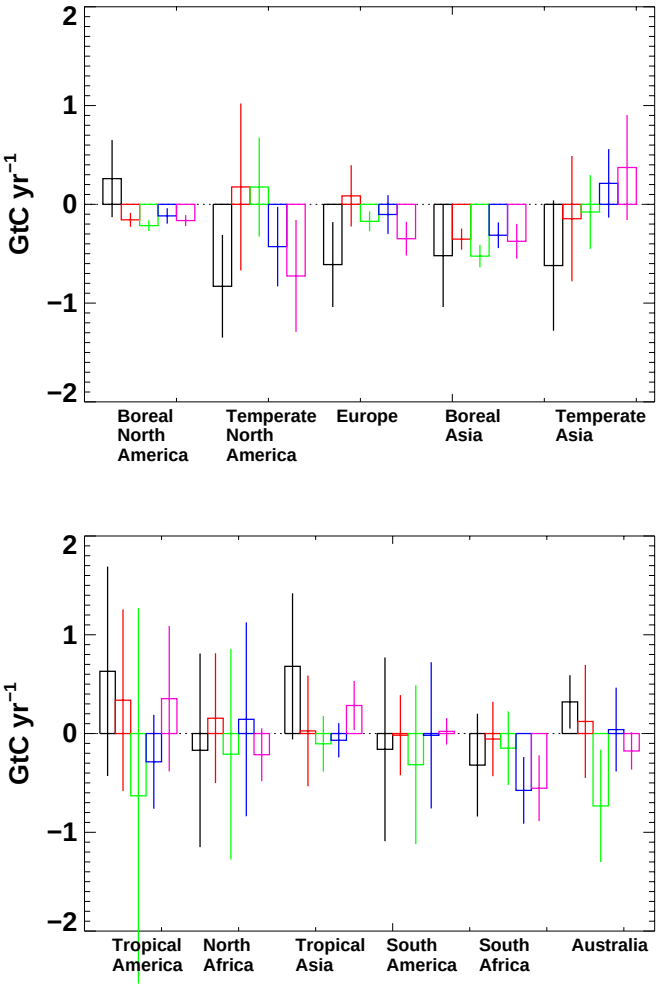

Figure 5.2. As fig 5.1, but for regional fluxes. The regions used are the same as defined by Gurney et al. (2002).

The conclusion is that the HadCM3LC experiments in general, and the C4MIP experiment in particular, are very good at simulating large scale regional carbon fluxes – especially on the global and semi-global scale. The model is also good at simulating smaller scale (continental and sub-continental) regional fluxes. But it must be remembered that as the size of the region decreases then so does the precision of the inversion estimate. It is likely that some of the differences between modelled and inversion results are also due to climatic and non-climatic influences of the Pinatubo eruption which cannot be simulated with this model configuration. There is also uncertainty in the regional distribution of land-use change carbon fluxes which must be added to the simulated fluxes before comparison with the inversion data.

6. Carbon budgets by country

It is interesting to see how modelled NEP varies on a country-by-country basis, although the data presented here are not directly comparable with any observed data. It must be remembered that the simulation takes no account of land-use change or fire disturbance which may both affect the biospheric carbon balance, particularly on a regional scale. Table 6.1 shows mean terrestrial uptake in the model for the 1980s, 1990s and whole of the 20th century for each of the countries listed. There are no data available of carbon fluxes on such a small scale (even continental flux estimates are still subject to much uncertainty, as discussed in section 5), but the data is of general interest and may be useful in the future if inversion studies become able to give higher resolution flux estimates. For comparison, the table also lists annual mean fossil fuel emissions during the 20th century. No data is listed for carbon fluxes associated with anthropogenic land-use change because this is not known with such a small regional precision.

Country	1980s NEP (GtC yr^{-1})	1990s NEP (GtC yr^{-1})	20th Century NEP (GtC yr^{-1})	20th Century mean fossil fuel emissions (GtC yr^{-1})
USA	0.2341	0.2663	0.0613	0.847
Germany	0.0124	0.0049	0.0041	0.156
Canada	0.1524	0.1940	0.0947	0.136
UK	0.0122	0.0057	0.0032	0.124
France	0.0123	0.0067	0.0057	0.091
Japan	0.0081	0.0112	0.0050	0.064
India	-0.0855	-0.1226	0.0264	0.056
Australia	-0.1624	0.1342	0.0164	0.022
Brazil	-0.0027	-0.0339	0.1357	0.018

Table 6.1. 1980s, 1990s and 20th century carbon budget by country for a few chosen countries. First 3 columns of numbers show mean modelled NEP for each country (positive implies uptake by the biosphere). The final column shows mean fossil fuel emissions for the 20th century for each country for comparison (positive implies emission to the atmosphere).

In agreement with the global total, NEP during the 20th century is positive for each country. There is also a clear upwards trend for most of the countries, with 1980s and 1990s NEP being greater than the 20th century mean, although inter-decadal variability leads to some countries having greater values for the 1980s than the 1990s. The exceptions here are India and Brazil where NEP has been negative for the last 20 years of the simulation.

7. Conclusions

An experiment with the atmospheric and terrestrial carbon cycle components of HadCM3LC has been performed, forced with observed SSTs, sea-ice and atmospheric CO_2 concentration.

The model's simulation of global mean temperature was close to observed, but this is not surprising given that the SSTs were prescribed. Regional temperature errors were found along with regional errors in precipitation: the model was often a little too cold and too wet over land areas.. On the global scale the model simulated a steady increase in GPP, R_P and R_S with a net positive NEP throughout the century which increased slightly during the century. The terrestrial uptake was partitioned roughly equally between storage in the vegetation and the soil, with soil accumulating more carbon in the early part of the century and vegetation more in the latter half. Very little change was simulated in terms of global mean vegetation fractions, although regionally there were some changes – trees and shrubs were out competing grass in South America and the Boreal regions respectively. However, given that the simulation did not include any anthropogenic changes in land-use, it is not generally possible to validate these changes against observations.

The model output was compared with point flux measurements from the CarboEurope network of towers. It was noticed that ecosystem respiration was persistently too large in the model both on a point by point basis and, to a lesser extent, as a function of temperature. However, it is difficult to make any firm conclusions on the basis of this given the many difficulties of comparing point observations with gridbox average values from the model. Simulated GPP was sometimes greater and sometimes smaller than observed. Simulated NEP was generally much lower in magnitude than observed. Most sites measured sinks, whereas the modelled NEP was generally much closer to zero. For some of the sites, differences in the simulated climate or land cover were responsible for the discrepancies, but generally it is likely that factors outside the scope of the model – in particular land use history and management practices (and also local topography and soil conditions) – are responsible for the observed widespread European carbon sink which is absent from the model results.

Simulated interannual variability in the global carbon fluxes was seen to be in good agreement with that expected in relation to the ENSO cycle – NEP was enhanced during La Nina events and reduced during El Nino events. Simulated terrestrial fluxes were in good agreement with observed changes in atmospheric CO_2 concentrations at Mauna Loa. Simulated terrestrial flux variability was greater in magnitude than interannual changes in CO_2, but this is expected because oceanic fluxes oppose the terrestrial fluxes and reduce the overall variability of observed CO_2. In agreement with previous studies, it was found that the majority of this signal was from the tropics, where it resulted from decreased uptake in El Nino events as a result of GPP being limited by reduced precipitation and respiration being increased as a result of the higher temperatures.

The model performed well on a regional scale when compared with flux estimates from the TransCom3 inversion study of Gurney et al. (2002). On the global and semi-global scale the agreement for the 1992-1996 period was very good, with the C4MIP experiment matching the inversion estimates more closely than previous fully coupled HadCM3LC experiments and well within the inversion uncertainties. When compared against smaller regions, there was more discrepancy between the

model and the inversion results. This may be partly due to errors in the simulated climate and carbon cycle on a regional scale, but may also be due to the larger uncertainty in the inversion results for small regions as compared with the global scale. The C4MIP results were generally closer to the inversion estimates than the other experiments, indicating the importance of being able to accurately simulate the climate.

This report assesses the ability of HadCM3LC to simulate the terrestrial carbon cycle changes during the 20th century when run under the protocol of the C4MIP phase 1 experiment. The model results have been compared with large and small spatial scale data and long and short timescale data and in general have shown that the model performs well. The intention of the C4MIP phase 1 experiment is to determine the extent of confidence we can have in model simulations of the 21st century. We found no large scale or persistent biases or errors in the model which may indicate that HadCM3LC is not suitable for such simulations.

References

Aubinet M., Grelle A., Ibrom A., Rannik U., Moncrieff J., Foken T., Kowalski AS., Martin PH., Berbigier P., Bernhofer C., Clement R., Elbers J., Granier A., Grunwald T., Morgenstern K., Pilegaard K., Rebmann C., Snijders W., Valentini R., Vesala T., Estimates of the annual net carbon and water exchange of forests: The EUROFLUX methodology. *Advances in Ecological Research*, **30**:113-175 2000.

Bousquet, P., P. Peylin, P . Ciais, C. Le Quere, P . Friedlingstein, and P.P. Tans. Regional changes in CO2 fluxes of land and ocean since 1980. *Science*, **290**:1342-1346, 2000.

Cox, P. M., Description of the TRIFFID dynamic global vegetation model, Technical Note 24, Hadley Centre, Met Office, 2001.

Cox, P. M., R. A. Betts, C. D. Jones, S. A. Spall, and I. J. Totterdell, Acceleration of global warming due to carbon-cycle feedbacks in a coupled climate model, *Nature*, **408**, 184-187, 2000.

Cox, P. M., R. A. Betts, C. D. Jones, S. A. Spall, and I. J. Totterdell, Modelling vegetation and the carbon cycle as interactive elements of the climate system, in *Meteorology at the Millennium*, edited by R. Pearce, pp. 259-279, Academic Press, 2001.

Francey, R. J., P.P. Tans, C.E. Allison, I.G. Enting, J.W.C . White, and M. Trollier. Changes in oceanic and terrestrial carbon uptake since 1982. *Nature*, **373**:326-330, 1995.

Friedlingstein, P., L. Bopp, P. Ciais, J. Dufresne, L. Fairhead, H. LeTreut, P. Monfray, and J. Orr, Positive feedback between future climate change and the carbon cycle, *Geophys. Res. Let*., **28**, 1543-1546, 2001.

Friedlingstein, P., J. L. Dufresne, P. M. Cox, and P. Rayner, How positive is the feedback between climate change and the carbon cycle?, *Tellus. B*, **55B**, 692-700, 2003.

Goldewijk, K. K.. Estimating global land use change over the past 300 years: The HYDE database. Global Biogeochem. Cycles, **15**(2):417-433, 2001.

Gu, L., D. D. Baldocchi, S. C. Wofsy, J. W. Munger, J. J. Michalsky, S. P. Urbanski, and T. A. Boden, Response of a deciduous forest to the Mount Pinatubo eruption: Enhanced photosynthesis, *Science*, **299**, 2035-2038, 2003.

Gurney, K. R., R. M. Law, A. S. Denning, P. J. Rayner, D. Baker, P. Bousquet, L. Bruhwiler, Y. H. Chen, P. Ciais, S. Fan, I. Y. Fung, M. Gloor, M. Heimann, K. Higuchi, J. John, T. Maki, S. Maksyutov, K. Masarie, P. Peylin, M. Prather, B. C. Pak, J. Randerson, J. Sarmiento, S. Taguchi, T. Takahashi, and C. W. Yuen, Towards robust regional estimates of CO_2 sources and sinks using atmospheric transport models, *Nature*, **415**, 626-630, 2002.

Jones, C. D., M. Collins, P. M. Cox, and S. A. Spall, The carbon cycle response to ENSO: A coupled climate-Carbon cycle model study, *J. Climate*., **14**, 4113-4129, 2001.

Jones, C. D. and P. M. Cox, Modelling the volcanic signal in the atmospheric CO record, *Global Biogeochem. Cycles*, **15**, 453-466, 2001.

Jones, C. D., P. M. Cox, R. L. H. Essery, D. L. Roberts, and M. J. Woodage, Strong carbon cycle feedbacks in a climate model with interactive CO_2 and sulphate aerosols, *Geophys. Res. Let*., **30**, 10.1029/2003GL016867, 2003.

Keeling, C. D., T.P. Whorf, M. Whalen, and J. Van der Plicht. Interannual extremes in the rate of rise of atmospheric carbon dioxide since 1980. *Nature*, **375**(6533):666-670, 1995.

Legates, D. R. and C. J. Willmott. Mean seasonal and spatial variability in global surface air temperature. *Theoretical and Applied Climatology*., **41**:11-21, 1990.

Lucht, W., I. C. Prentice, R. B. Myneni, S. Sitch, P. Friedlingstein, W. Cramer, P. Bousquet, W. Buermann, and B. Smith, Climatic control of the high-latitude vegetation greening trend and Pinatubo effect, *Science*, **296**, 1687-1689, 2002.

Prentice, I., G. Farquhar, M. Fasham, M. Goulden, M. Heimann, V. Jaramillo, H. Kheshgi, C. Le Quere, R. Scholes, and D. Wallace, The carbon cycle and atmospheric carbon dioxide, in *Climate Change 2001: The scientific basis. Contribution of Working Group I to the Third Assessment Report of the Intergovernmental Panel on Climate Change*, edited by J. T. Houghton, Y. Ding, D. J. Griggs, M. Noguer, P. van der Linden, X. Dai, K. Maskell, and C. I. Johnson, chapter 3, pp. 183-237, Cambridge University Press, 2001.

Ramankutty, N. and J. A. Foley, Estimating historical changes in global land cover: Croplands from 1700 to 1992. *Global Biogeochem. Cycles*, **13**:997-1027, 1999.

Rayner, N. A., D. E. Parker, E. B. Horton, C. K. Folland, L. V. Alexander, D. P. Rowell, E. C. Kent, and A. Kaplan, Global analyses of SST, sea ice and night marine air temperature since the late nineteenth century, *J. Geophys. Res*., **108**, 10.1029/2002JD002670, 2003.

Sturm M., C. Racine, K. Tape, Climate change: Increasing shrub abundance in the Arctic, *Nature*, **411**: 546-547, 2001.

Thornton, P. E., B. E. Law, H. L. Gholz, K. L. Clark, E. Falge, D. S. Ellsworth, A. H. Goldstein, R. K. Monson, D. Hollinger, M. Falk, J. Chen, J. P. Sparks, Modeling and measuring the effects of disturbance history and climate on carbon and water budgets in evergreen needleleaf forests, *Agric. And Forest Met.*, **113**, pp. 185-222, 2002.

Tucker C. J., Slayback D. A., Pinzon J. E., Los S. O., Myneni R. B., Taylor M. G., Higher northern latitude normalized difference vegetation index and growing season trends from 1982 to 1999, *International Journal of Biometeorology* **45**(4): 184-190, 2001.

Valentini R. (ed.) 2003. Fluxes of carbon, water and energy of European forests. *Ecological Studies,* **163**, pp. 270.

Xie, P. and P. A. Arkin. Global precipitation: A 17-year monthly analysis based on gauge observations, satellite estimates and numerical model outputs. *Bull. Am. Meteorol. Soc*., **78**:2539-2558, 1997.

Zeng, N., A. Mariotti and P. Wetzel, Mechanisms of Interannual CO_2 Variability, *Global Biogeochem. Cycles*, submitted, 2004a.

Zeng, N., H. Qian, E. Munoz, and R. Iacono, How strong is carbon cycle-climate feedback under global warming?, Geophys. Res. Lett., **31**, L20203, doi:10.1029/2004GL020904, 2004b.

Zhou L. M., Tucker C. J., Kaufmann R. K., Slayback D., Shabanov N. V., Myneni R. B., Variations in northern vegetation activity inferred from satellite data of vegetation index during 1981 to 1999, *J. Geophys. Res. (Atm.)* **106**: 20069-20083, 2001.